2023 年 9 月　　岩　矿　测　试　　Vol. 42, No. 5
September 2023　　ROCK AND MINERAL ANALYSIS　　888−902

白宇, 阿依努尔·吾舒尔, 欧阳磊, 等. 羧基功能化共价膦腈聚合物用于酸性水体中钪的选择性分离[J]. 岩矿测试, 2023, 42(5): 888−902. doi: 10.15898/j.ykcs.202307290098.

BAI Yu, WUSHUER Ayinuer, OUYANG Lei, et al. Selective Separation of Scandium in Acidic Water Using Carboxyl Functionalized Covalent Phosphonitrile Polymers[J]. Rock and Mineral Analysis, 2023, 42(5): 888−902. doi: 10.15898/j.ykcs.202307290098.

羧基功能化共价膦腈聚合物用于酸性水体中钪的选择性分离

白宇[1,2]，阿依努尔·吾舒尔[1]，欧阳磊[1]，黄理金[1,3*]，帅琴[1,3]
(1. 中国地质大学(武汉)材料与化学学院，湖北 武汉 430074；
2. 浙江省地矿科技有限公司，浙江 杭州 310007；
3. 自然资源部稀土稀有稀散矿产重点实验室，湖北 武汉 430034)

摘要：发展高效选择性分离技术实现酸性介质中稀土元素钪(Sc)的高效提取，有利于满足工业生产过程对Sc日益增长的需求。吸附法可以有效地简化Sc的提取流程，降低生产成本。然而，现有吸附材料如硅基材料、生物质材料、金属有机骨架材料等在分离酸性介质中的Sc时仍存在效率低、选择性差等缺点，从而限制了其实际应用。因此，针对处理含Sc尾矿等原料时往往需要进行酸处理的实际情况，制备具备更强结合能力的吸附剂，实现酸性介质中Sc(III)的高效选择性分离至关重要。本文分别以间苯三酚和2,4,6-三羟基苯甲酸为构筑单元，与六氯三聚膦腈共价交联制备了共价膦腈聚合物(covalent phosphonitrile frameworks，CPF-T)和羧基功能化CPF材料(CPF-T-COOH)。采用扫描电镜、红外光谱、热重、氮气吸附-解吸等分析技术对材料的结构进行表征，并探索了它们作为Sc(III)吸附剂的应用潜力。吸附实验结果表明，在溶液pH=2时，CPF-T和CPF—COOH对Sc(III)的吸附平衡时间分别为120min和30min，最大吸附容量分别为22.48mg/g和64.63mg/g，在混合离子溶液中的分配系数分别为5.1×10^{2}mL/g和4.0×10^{3}mL/g。值得注意的是，在酸性介质(pH=1～3)中，CPF-T-COOH对Sc(III)的吸附率仍维持在95%以上，明显优于CPF-T(低于60%)以及大多数已报道的吸附材料。采用X射线光电子能谱对作用机理进一步分析，结果显示除了CPF-T骨架中N/O原子与Sc(III)的配位作用外，骨架—COOH上的O原子与-OH基团分别提供了额外的配位作用与离子交换作用，有效地增强了CPF—COOH对Sc(III)的吸附亲和力。该研究表明，利用多种功能基团的协同作用是提高吸附剂吸附性能的有效策略之一，所制备的CPF-T-COOH材料性能优异，展现了其作为Sc(III)吸附材料的良好应用前景。

关键词：钪；共价膦腈聚合物；选择性分离；协同效应；X射线光电子能谱

要点：

(1)羧基修饰的共价膦腈聚合物可实现酸性介质中Sc(Ⅲ)的高效选择性分离。

(2)—COOH修饰共价膦腈聚合物吸附Sc(III)的主要作用机制是配位和离子交换作用。

(3)多种功能基团的协同作用有效地增强了共价膦腈聚合物对Sc(III)的结合能力。

中图分类号：P618.7　　**文献标识码：**A

收稿日期：2023−07−29；**修回日期：**2023−08−23；**接受日期：**2023−09−01

基金项目：国家重点研发计划项目(2021YFC2903000)课题“战略性矿产微区原位分析技术及应用”；自然资源部稀土稀有稀散矿产重点实验室开放基金资助项目(KLRM-KF202006)；自然资源部离子型稀土资源与环境重点实验室开放基金资助项目(2022IRERE304)

第一作者：白宇，硕士研究生，分析化学专业。E-mail：ybai@cug.edu.cn。

通信作者：黄理金，博士，副研究员，主要从事先进功能材料绿色制备及其分离分析应用研究。
E-mail：huanglj@cug.edu.cn。

钪(Sc)与钇、镧系、锕系元素共称为稀土元素,是被认为最有价值的稀土元素之一,截至 2021 年底,Sc_2O_3 的价格为$900/kg,纯金属价格为$3000/kg[1-3]。Sc 以其自身的高熔点、高沸点、低密度、稳定性好等优良的性能成为许多先进制造业中一种不可或缺的元素。例如,卤化物灯和铝合金的生产[4]、高性能陶瓷的合成[5]、钙钛矿氧化物电极性能的改善[6]等。虽然 Sc 的地壳平均丰度为 22μg/g,但是 Sc 作为一种典型的分散元素,通常以伴生矿产存在,需要从生产其他金属的矿石(如铝矿石、钛矿石、钨矿石等)残留物和尾矿副产品、含 Sc 内(外)生矿床中生产主产品的过程中回收,或从工业废水、废渣中进行回收[7-8]。Sc 提取和回收过程中存在回收率低、操作复杂等问题,使其越来越无法满足社会发展对其日益增长的需求,因此,亟需开发有效地回收 Sc 的方法。目前分离 Sc 的方法有化学沉淀法[9]、液膜分离法[10]、溶剂萃取法[11-13]、吸附法[14-15]等。吸附法因具有操作简便、成本低、回收率高等优势,已经逐步发展为一种有效的回收 Sc 的技术。目前,常被用于分离 Sc(III)的吸附剂包括硅基材料(如 SAB-15)[5, 16-17]、生物材料[9]、金属有机骨架材料[18]等。虽然这些材料在一定程度上对 Sc(III)表现出良好的吸附能力,但是这些吸附剂固有的结构缺点包括化学稳定性差和往往依赖一种功能基团作为吸附位点,导致它们适用的 pH 范围有限,吸附容量和选择性也存在较大的提升空间。由于处理含 Sc 尾矿等原料时往往需要采用盐酸、硝酸或硫酸等强酸进行处理[19-20],因此发展能够在酸性介质中高效选择性地回收 Sc(III)的吸附剂至关重要。

共价有机聚合物是一类以共价键连接的多孔有机材料。由于其可调的化学结构,可以针对目标离子特性灵活调控材料的孔径尺寸、功能基团类型和密度,共价有机聚合物是一类具有良好发展前景的吸附材料[21-23]。酸性介质中官能团质子化所引起的与阳离子目标物之间的静电排斥效应是导致大多数材料吸附性能下降的主要原因之一。基于孔径尺寸匹配的物理作用可以在一定程度上解决酸性介质中官能团失效的问题,从而实现酸性体系中目标离子的选择性吸附[24-25]。但是由于目前合成的绝大多数的共价有机聚合物的孔径尺寸远大于金属离子的尺寸,因此该方法一般只适用于尺寸较大的离子,如水合铀离子。通过离子印迹技术[26]或者选择与目标离子具有尺寸匹配空腔的单体制备共价有机聚合物可以解决这一问题[27],但是在一定程度上增加了材料合成的复杂性。对于共价有机聚合物,修饰官能团也是提高吸附剂吸附性能的另一种重要方法。例如,在材料中引入含 S 官能团如-SH[28]、C=S[29],可以有效地提高其对 Hg(II)的吸附能力。这一方法主要根据 Lewis 软硬酸碱理论实现,即在材料骨架结构中引入含有与目标离子软硬性相近的功能基团。对于硬酸性稀土离子,P-O[30]、$-NH_2$[31]等硬碱性化学键与之具有强配位作用。为了解决单一功能基团修饰存在的吸附亲和力受限的问题,采用加入多种不同功能基团的萃取剂或在材料中引入两个或多个不同的功能基团,利用不同基团之间存在的协同作用,可有效地提升材料对于靶向目标离子的选择性结合能力[32-33]。

Zhang 等[24]报道的共价膦腈聚合物(covalent phosphonitrile framework, CPF-T)的骨架中含有丰富的硬碱性含 N/O 的基团,理论上是对硬酸性离子 Sc(III)的有效吸附剂。本文在 CPF-T 基础之上进一步引入与稀土具有强相互作用的—COOH 功能基团,制备羧基功能化材料 CPF-T-COOH,以探究功能基团—COOH 引入后,材料对 Sc(III)吸附效果的影响。采用傅里叶变换红外光谱(FT-IR)、热重分析(TGA)、扫描电子显微镜(SEM)、氮气吸附-解吸实验对材料的结构进行了表征。通过静态吸附实验对比了 CPF-T 与 CPF-T-COOH 对 Sc(III)吸附性能的差异,包括溶液 pH 的影响、吸附动力学、吸附等温线、吸附选择性。最后,通过 X 射线光电子能谱(XPS)表征进一步探讨了 CPF-T-COOH 吸附 Sc(III)的作用机理。这项研究有望为金属离子高效吸附剂的设计合成提供理论依据。

1　实验部分

1.1　主要试剂

六氯三聚膦腈(HCCP)、无水间苯三酚、三乙胺:购自上海阿拉丁生物科技股份有限公司。2,4,6-三羟基苯甲酸:购自源叶生物科技有限公司。1,4-二氧六环、硝酸钪:购自上海麦克林生化科技有限公司。

无水乙醇、氢氧化钠、硝酸、丙酮、硝酸铝、硝酸钙、硝酸铜、硝酸钴、硝酸锰、硝酸锌:购自国药集团化学试剂有限公司。硫酸镁:购自永华化学科技(江苏)有限公司。

以上试剂为分析纯,未经纯化后直接使用。

1.2　吸附材料制备

按照 Zhang 等[24]报道的方法制备 CPF-T,主要步骤如下:将 1mmol 间苯三酚和 0.5mmol HCCP

溶解于 1mL 的 1,4-二氧六环中使之形成透明溶液，随后加入 0.84mL 三乙胺。将此混合物转移至 8mL 水热反应釜中，在 80℃ 下反应 24h。将产物用水、乙醇、丙酮洗涤几次。最后在 50℃ 下真空干燥 12h 制得淡粉色粉末状的 CPF-T。将间苯三酚替换为 2,4,6-三羟基苯甲酸，按照同样步骤制备 CPF-T-COOH，产物为淡粉色粉末。图 1 为材料制备化学反应式，基于酚-OH 与-Cl 之间的取代反应，使分子交联形成聚合物，在此基础之上将—COOH 引入结构骨架中。

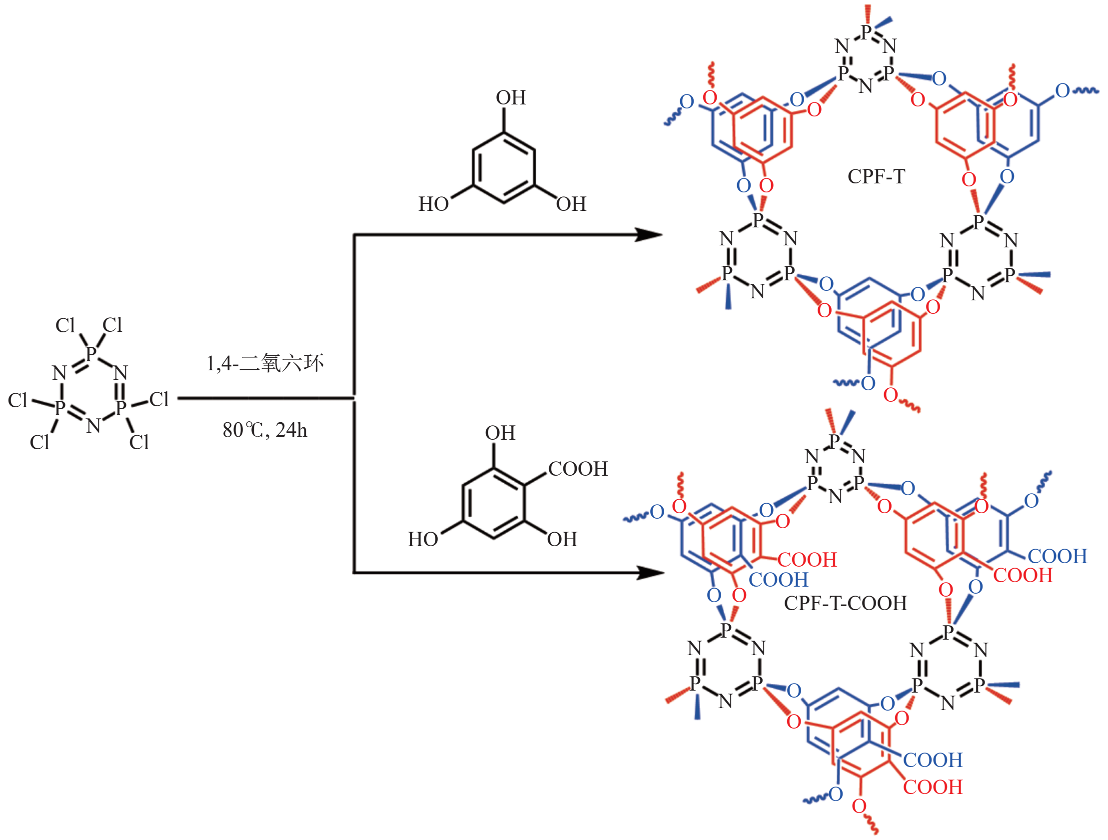

图1　共价膦腈聚合物 CPF-T 和羧基功能化材料 CPF-T-COOH 制备化学反应式

Fig. 1　Hexachlorotriphosphazene crosslinked with phloroglucinol and 2,4,6-trihydroxybenzoic acid to prepare covalent phosphonitrile framework (CPF-T) and carboxyl modified CPF-T-COOH.

1.3　吸附实验主要流程

将硝酸钪溶于 2% 硝酸中配制 Sc(III)的标准溶液，浓度为 1000mg/L。使用 0.1mol/L 硝酸和 0.1mol/L 氢氧化钠溶液调节溶液的 pH，过程中使用 pH 计进行监测。以 10mL 离心管为容器，在室温下通过恒温振荡器(150r/min)进行吸附实验，吸附剂用量为 1g/L，实验数据取 3 组平行实验的平均值。振荡结束后，经 0.45μm 微孔滤膜过滤后得到清液经 EXPEC 6000 型电感耦合等离子体发射光谱仪(杭州谱育科技发展有限公司)测试，标准曲线方程 $R^2>0.999$。

1.4　材料表征方法

为了验证聚合物的成功制备，通过溴化钾压片法制样，经 Thermo Scientific Nicolet iS20 傅里叶变换红外光谱(FT-IR，美国 ThermoFisher 公司)采集聚合物的红外光谱图以获取其分子结构信息。

使用 SU8010 型扫描电子显微镜(SEM，日本日立公司)观测两种聚合物的微观形貌。

经 DTA7200 型热重分析仪(TGA，日本日立公司)在氮气条件下(流速 20mL/min；加热速度 10K/min)采集聚合物的 TGA 曲线。

为了分析材料的元素信息，通过 Thermo Scientific K-Alpha 型 X 射线光电子能谱(XPS，美国 ThermoFisher 公司)对聚合物进行表征，激发源为 Al Kα 射线($h\nu$=1486.6eV)，光斑大小为 400μm，工作电压为 12kV，灯丝电流为 6mA。

为了得到材料的比表面积和孔结构信息, 使用 Micromeritics APSP2460 型 4 站式全自动比表面积分析仪(美国 Micromeritics 公司)在 77K 下测得材料的氮气吸附-脱附等温线, 测定前将样品在 120℃ 下真空脱气 12h。

1.5　数据分析与处理

使用专业软件 Advantage 对 XPS 数据进行处理得到材料的元素含量和 N、O 元素的形态, 在分峰拟合前, 以 C1s(284.8eV)为标准进行电荷校正。

在吸附实验中, 吸附率、吸附容量(q_e, mg/g)、分配系数 K_d 分别由以下式(1)、式(2)、式(3)计算:

$$\text{吸附率} = \frac{c_0 - c_e}{c_0} \times 100\% \tag{1}$$

$$q_e = \frac{c_0 - c_e}{m} \times V \tag{2}$$

$$K_d = \frac{c_0 - c_e}{c_e} \times \frac{V \cdot 10^3}{m} \tag{3}$$

式中: c_0 为待吸附溶液中 Sc(III)的初始浓度(mg/L); c_e 为达到吸附平衡时, 溶液中 Sc(III)的残留浓度(mg/L); V 为溶液体积(L); m 为吸附剂的质量(g)。

FT-IR 图、氮气吸附-脱附等温线、TGA 曲线及以上所有得到的数据经 Origin 软件进行图的制作, 图中误差棒为标准偏差。

2　结果与讨论

2.1　制备材料表征结果分析

2.1.1　FT-IR 特征

在 CPF-T 和 CPF-T-COOH 红外谱图(图 2a)中, 1235cm^{-1}(1243cm^{-1})和 862cm^{-1}(837cm^{-1})处分别为 HCCP 中 P=N 和 P-N 的伸缩振动峰[24, 34]。在 CPF-T-COOH 的红外谱图中, 1644cm^{-1} 处为—COOH 中 C=O 双键的伸缩振动峰; 1476cm^{-1} 为—COOH 中 C-O 单键的特征吸收峰, 约 3400cm^{-1} 处为-OH 的伸缩振动峰; 2681cm^{-1} 为 Ar-C 的特征峰[14]。同时, 在两种材料的 FT-IR 谱图中, 都观测到 P-O-Ar 的伸缩振动峰, 即 CPF-T: 1020cm^{-1} 和 CPF-T-COOH: 1012cm^{-1}[24]。FT-IR 表征结果表明有机单体 HCCP 与间苯三酚、2,4,6-三羟基苯甲酸成功交联, 得到了 CPF-T 和 CPF-T-COOH。

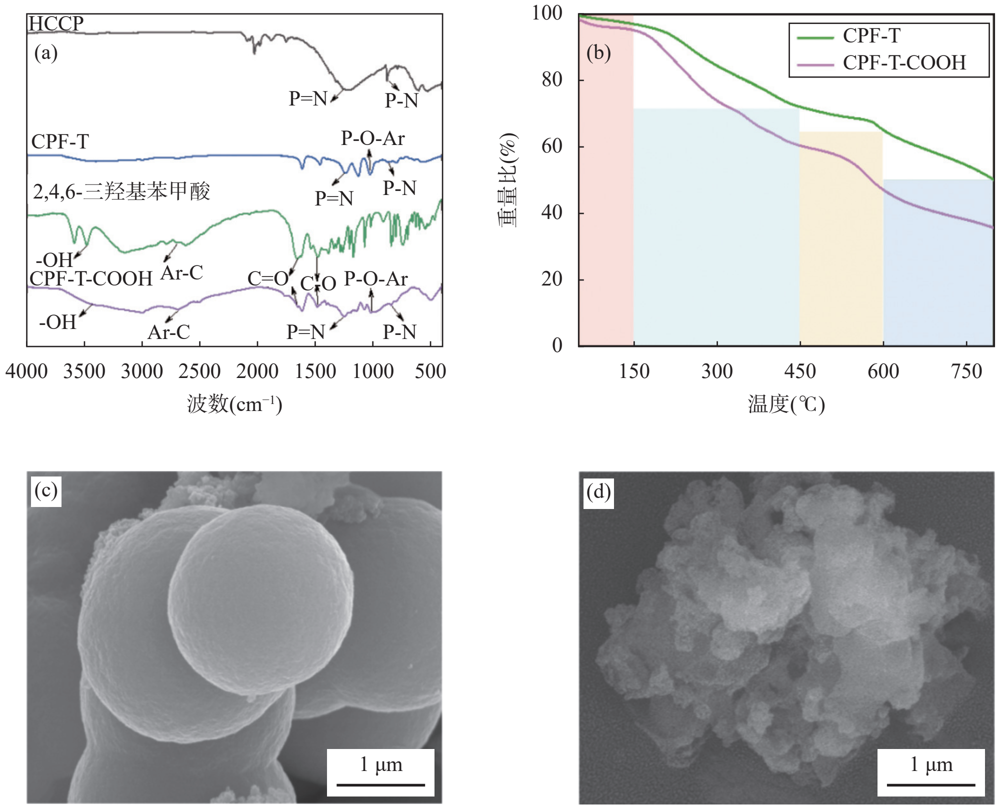

图2　CPF-T、CPF-T-COOH、HCCP、2, 4, 6-三羟基苯甲酸的 FT-IR 谱图 (a); CPF-T 和 CPF-T-COOH 的 TGA 曲线 (b); CPF-T (c) 和 CPF-T-COOH (d) 的 SEM 图像

Fig. 2　FT-IR spectra of CPF-T, CPF-T-COOH, HCCP and 2, 4, 6-trihydroxybenzoic acid (a); TGA curves of CPF-T and CPF-T-COOH (b); SEM images of CPF-T (c) and CPF-T-COOH (d).

2.1.2 热稳定性

通过 TGA 分析了 CPF-T 和 CPF-T-COOH 的热稳定性，两种材料的 TGA 曲线如图 2b 所示。材料的 TGA 曲线可以被分成四个失重阶段：低于 150℃为第一阶段，150～450℃为第二阶段，450～600℃为第三阶段，高于 600℃为第四阶段。在第一阶段两种材料较稳定，其质量损失很少，可能是由于有机溶剂和吸附水的蒸发引起的。在第二阶段，CPF-T 和 CPF-T-COOH 的质量损失约为 25% 和 35%，可能是因为膦腈环的裂解[35]和 CPF-T-COOH 发生了脱羧反应[36]。在第三阶段，CPF-T 和 CPF-T-COOH 的质量损失率较小，分别为 7% 和 13% 左右，可归因于 P-O 键的断裂[24]。在第四阶段，两种材料的质量损失可能是由材料中剩余部分，如苯环等发生碳化引起的[24]。总之，CPF-T 和 CPF-T-COOH 均具有较好的热稳定性。

2.1.3 微观形貌

通过 SEM 表征考察了 CPF-T 和 CPF-T-COOH 的微观形貌。由图 2c 观察到 CPF-T 呈现表面较为光滑的球状结构，部分发生团聚。由图 2d 观察到 CPF-T-COOH 呈不规则的、类“蚁穴”多孔结构，表面较为粗糙。

2.1.4 孔隙率和比表面积

为了分析 CPF-T 和 CPF-T-COOH 的孔结构和比表面积，本文对材料进行了氮气吸附-脱附实验。CPF-T 和 CPF-T-COOH 的氮气吸附-脱附等温线如图 3 所示。根据 IUPAC 的分类，CPF-T（图 3a）和 CPF-T-COOH（图 3b）的氮气吸附-脱附等温线属于 II 型，且在 P/P_0=0.8～1.0 范围内有强吸收，表明材料中存在微孔和介孔结构[37-38]。根据 BET 方程分别计算得到 CPF-T 和 CPF-T-COOH 的比表面积和总孔隙体积。CPF-T 的比表面积为 76.5m^2/g，总孔隙体积为 0.38cm^3/g；CPF-T-COOH 的比表面积为 2.61m^2/g，总孔隙体积为 0.035cm^3/g。与 CPF-T 相比，CPF-T-COOH 比表面积和总孔隙体积变小，可能是引入的羧基堵塞了材料的孔道[39]。

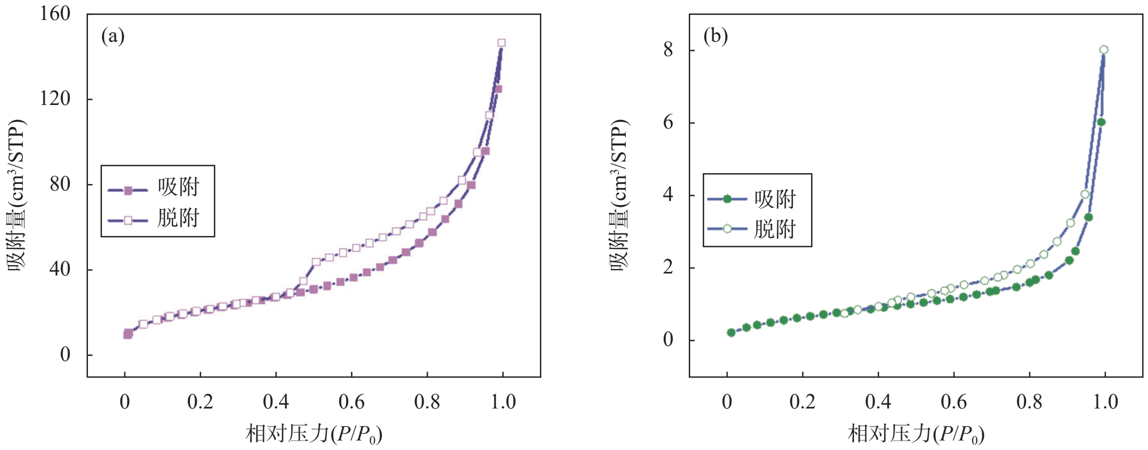

图3 CPF-T (a) 和 CPF-T-COOH (b) 的氮气吸附-脱附等温线

Fig. 3 Nitrogen adsorption-desorption isotherms of CPF-T (a) and CPF-T-COOH (b).

2.2 吸附实验吸附性能结果

为了研究 CPF-T 和 CPF-T-COOH 的吸附性能，分别进行了溶液 pH 的影响、吸附动力学、吸附等温线、吸附选择性测试实验。

2.2.1 溶液 pH 对吸附率的影响

溶液的 pH 对金属离子吸附效果起到关键作用[40-41]，故首先研究了溶液 pH 对两种材料吸附 Sc(Ⅲ)的影响。如图 4a 所示，两种材料对 Sc(Ⅲ)的吸附率随溶液 pH 的变化趋势不同。在 pH=6 时，CPF-T 对 Sc(Ⅲ)的吸附率达到 99%以上，但随着溶液酸性的增加，材料的吸附能力逐渐减弱。当溶液 pH=1 时，CPF-T 对 Sc(Ⅲ)的吸附率降低至 41%，可能的原因是因为 CPF-T 上的部分官能团随着溶液酸度的增加而质子化，在静电排斥作用下，正电形式的 Sc^{3+}难以接近吸附剂的表面[42]。然而，在溶液 pH=1～3 的范围内，CPF-T-COOH 对 Sc(Ⅲ)的吸附率均在 95%以上，表明羧基的引入有效地增强了材料与 Sc(Ⅲ)的结合能力。值得注意的是，之前报道的许多吸附剂在溶液 pH<2 时，失去了对 Sc(Ⅲ)的吸附能力或吸附率显著降低[10, 14-15, 43-44]，但是 CPF-

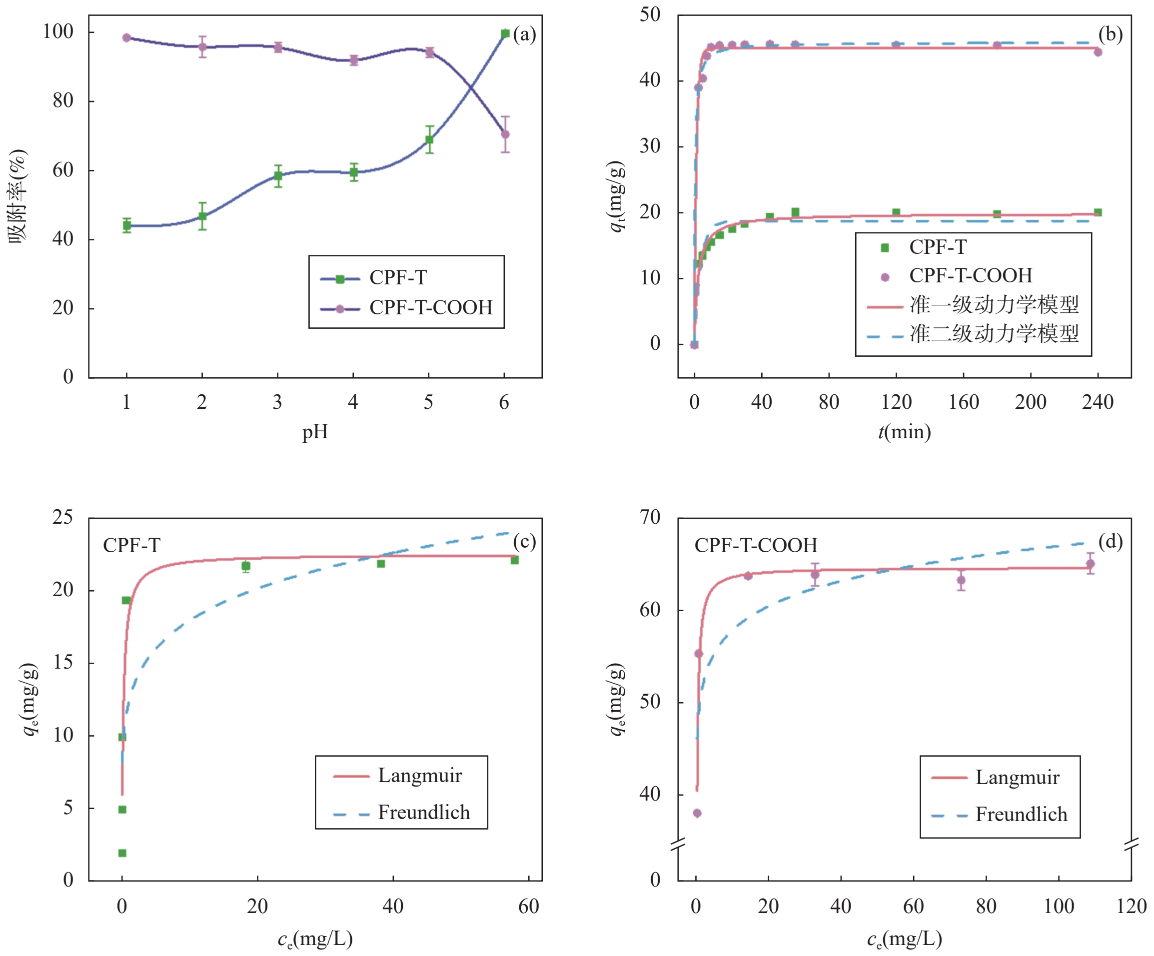

a—吸附剂用量 1g/L，温度 25℃，c_0 (Sc)=50mg/L；b—pH=2，吸附剂用量 1g/L，温度 25℃，c_0 (Sc)=50mg/L；c，d—pH=2，吸附剂用量 1g/L，温度 25℃。

图4　溶液 pH 对 CPF-T 和 CPF-T-COOH 吸附 Sc (III) 的影响 (a)；吸附动力学及准一级和准二级动力学拟合曲线 (b)；CPF-T (c) 和 CPF-T-COOH (d) 的吸附等温线及 Langmuir 和 Freundlich 模型拟合曲线

Fig. 4　The effect of solution pH on the adsorption of Sc (III) by CPF-T and CPF-T-COOH (a) (Adsorbent dosage: 1g/L; Temperature: 25℃; c_0 (Sc)=50mg/L); The adsorption kinetics and fitting curves of pseudo-first-order kinetic and pseudo-second-order kinetic (b) (pH=2; Adsorbent dosage: 1g/L; Temperature: 25℃; c_0 (Sc)=50mg/L); The adsorption isotherms of CPF-T (c) and CPF-T-COOH (d) and the fitting curves of the Langmuir and Freundlich models (pH=2; Adsorbent dosage: 1g/L; Temperature: 25℃).

T-COOH 在酸性体系中却表现出高吸附率，显示出其在酸性体系中回收 Sc(III)的应用潜力。

2.2.2　吸附平衡时间对比

为了探究两种吸附剂对 Sc(III)的吸附平衡时间与动力学机制，对吸附动力学进行了考察，结果如图 4b 所示。CPF-T 和 CPF-T-COOH 对 Sc(III)的吸附速率呈现先快速增加，之后速率变缓，当最后到达吸附平衡时，保持不变的趋势。CPF-T 的吸附过程在 120min 内才能到达吸附平衡，而 CPF-T-COOH 在 30min 内就能到达到吸附平衡。虽然 CPF-T-COOH 的比表面积小于 CPF-T，但由于其与 Sc(III)的作用力更强，因此吸附速率更快，吸附容量更高。分别采用准一级动力学(式 4)和准二级动力学模型(式 5)对实验数据进行拟合，拟合结果如表 1 所示。两种材料的准二级动力学模型的相关系数均大于准一级模型，因此在 CPF-T 和 CPF-T-COOH 吸附 Sc(III)的过程中，活性位点吸附为速控步[45-47]。

$$\log(q_e - q_t) = \log q_e - \frac{K_1}{2.303} \tag{4}$$

$$\frac{t}{q_t} = \frac{t}{q_e} + \frac{1}{K_2 q_e^2} \tag{5}$$

式中：q_t指t时刻材料对Sc(III)的吸附容量(mg/g)，q_e代表平衡吸附容量(mg/g)，K_1和K_2分别为准一级和准二级动力学模型的吸附速率常数，单位分别为min^{-1}和g/(mg·min)。

2.2.3 最大吸附容量对比

对CPF-T和CPF-T-COOH两种材料吸附Sc(III)的吸附等温线进行探究，结果分别如图4中c和d所示，可以看到CPF-T-COOH的最大吸附容量明显高于CPF-T。分别采用Langmuir(式6)和Freundlich(式7)模型对数据进行拟合，拟合结果如表2所示。两种材料的Langmuir模型的R^2值都高于Freundlich模型，说明吸附过程为单层吸附[47-48]。Langmuir模型拟合得到的CPF-T和CPF-T-COOH对Sc(III)的最大吸附容量分别为22.48mg/g和64.63mg/g。另外，在Langmuir模型拟合参数中，CPF-T-COOH的K_L值约为CPF-T的1.5倍，说明CPF-T-COOH与Sc(III)的吸附亲和力更高[49-50]。

$$\frac{c_e}{q_e}=\frac{1}{q_m K_1}+\frac{c_e}{q_m} \tag{6}$$

$$\log q_e=\log K_f+\frac{1}{n}\log c_e \tag{7}$$

式中：q_m代表对Sc(III)的最大吸附容量(mg/g)，c_e是达到吸附平衡时，溶液中Sc(III)的浓度(mg/L)；K_L为Langmuir常数(L/mg)；n为Freundlich经验参数，K_f为Freundlich常数[(mg/g)·(mg/L)$^{-1/n}$]。

2.2.4 吸附选择性

为了探究CPF-T和CPF-T-COOH对Sc(III)的吸附选择性，进行了Mg(II)、Co(II)、Mn(II)、Ca(II)、Al(III)、Cu(II)、Zn(II)存在条件下的共存离子实验。根据图5可知，两种材料都具有选择性吸附Sc(III)的能力，对Sc(III)的K_d值分别为5.1×10^2mL/g和4.0×10^3mL/g。CPF-T-COOH的吸附选择性高于CPF-T，这可能是多功能位点协同作用的结果(在2.3节中进一步讨论)。总的来说，CPF-T-COOH对Sc(III)具有较好的吸附选择性，在实际应用中具有选择性回收和分离Sc(III)的潜力。

2.2.5 与已报道材料的吸附性能对比

表3列举了一些已报道的吸附剂与CPF-T-COOH对Sc(III)的在固定溶液pH下的吸附平衡时间和最大吸附容量。大部分吸附剂的最佳pH为5左右，而CPF-T-COOH可以在pH=2的介质中吸附>95%的Sc(III)，相比其他吸附剂具有更广泛的pH适用范围。CPF-T-COOH的最大吸附容量处于中间水平，但是其吸附平衡时间与其他吸附剂相比是最短的。在Langmuir吸附等温线模型中，K_L值越大表示与目标物的吸附亲和力越强[49-50]，CPF-T-COOH的K_f值是其他吸附剂的10倍以上，在高亲和力的驱动下，使得其具有更快的吸附动力学，到达平衡所需时间更短，而且在酸性介质中的吸附性能得到有效提高。

2.3 吸附机理分析

为了探究CPF-T-COOH对Sc(III)的作用机理，对吸附前后的材料进行了XPS表征。有研究表明，与P相连接的N、O原子表现出硬碱性，对稀土离子具有强配位作用[24, 30]。此外，—COOH除了可以

表1 CPF-T和CPF-T-COOH吸附Sc (III)的准一级和准二级动力学模型拟合参数

Table 1 The fitting parameters of the pseudo first-order and the pseudo second-order kinetic models for the adsorption of Sc (III) by CPF-T and CPF-T-COOH.

吸附剂	准一级动力学模型			准二级动力学模型		
	K_1 (min^{-1})	q_{e1} (mg/g)	R^2	K_2 [g/(mg·min)]	q_{e2} (mg/g)	R^2
CPF-T	0.1475	18.38	0.93	0.01195	19.83	0.98
CPF-T-COOH	0.3693	44.42	0.99	0.02216	46.78	1.0

表2 CPF-T和CPF-T-COOH吸附Sc(III)的Langmuir和Freundlich等温线模型拟合参数

Table 2 The fitting parameters of the Langmuir and Freundlich models for the adsorption of Sc(III) by CPF-T and CPF-T-COOH.

吸附剂	Langmuir等温线模型			Freundlich等温线模型		
	K_L (L/mg)	q_{max} (mg/g)	R^2	K_f [(mg/g)·(mg/L)$^{-1/n}$]	n	R^2
CPF-T	4.099	22.48	0.93	12.21	5.998	0.74
CPF-T-COOH	5.994	64.63	0.96	49.97	15.74	0.74

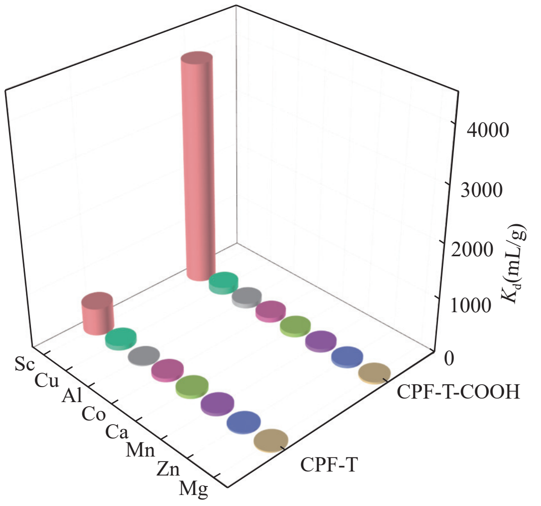

实验条件：pH=2，吸附剂用量 1g/L，温度 25℃，c_0=50mg/L。

图5　CPF-T 和 CPF-T-COOH 在共存离子实验中对金属离子的 K_d 值

Fig. 5　The K_d value of metal ions by CPF-T and CPF-T-COOH in coexisting ion experiments (Conditions: pH=2; Adsorbent dosage: 1g/L; Temperature: 25℃; c_0=50mg/L).

通过 O 与 Sc(III)进行配位外[54]，还可以通过离子交换作用与之形成羟基内核[14, 55]。故对 N 和 O 的 XPS 窄谱进行了详细分析，以明确这些可能的吸附作用机制。

虽然 Sc2p 与 N1s 的结合能相近，但在吸附后 N1s 的 XPS 谱图(图 6a)中观测到明显的属于 $Sc2p_{3/2}$(408.1eV)和 $Sc2p_{1/2}$(400.8eV)的特征峰[43]，证明 Sc(III)被 CPF-T-COOH 成功捕获。图 6a 显示 N1s 包括三种化学形态，分别为 P-NH-P(398.0eV)、P=N-H(399.3eV)和 P-NH_2(401.6eV)[24]。吸附 Sc(III)后，三种峰的结合能均有所升高，偏移至 398.1eV、399.6eV、403.5eV。这是由于 N 与 Sc(III)之间的配位作用导致的，即 N 原子中的孤对电子被贡献给 N 原子和 Sc(III)之间形成的配位键中，导致 N 原子的电子云密度降低，结合能增加[56]。

图 6b 显示材料吸附 Sc(III)前 O1s 有四种化学形态，分别为 C=O(534.2eV)[57]、C-OH(533.2eV)、

表 3　CPF-T-COOH 与部分已报道的 Sc (III) 吸附剂性能 (最佳 pH、吸附平衡时间、最大吸附容量、K_L 值) 对比

Table 3　Comparison of Sc (III) adsorption performance (the optimal pH, adsorption equilibrium time, maximum adsorption capacity, and the value of K_L) between CPF-T-COOH and some reported adsorbents.

材料名称	溶液 pH	吸附平衡时间 (h)	最大吸附容量 (mg/g)	K_L (mL/g)	参考文献
0.075-AA-0.072@MIL-101	4.5	5	90.21	1.7×10^5	[14]
BT/$CoFe_2O_4$@SiO_2-CMC/PAN	5	5	49.05	2.9×10^5	[43]
IIPBT/$CoFe_2O_4$@SiO_2	5	2	128	-	[51]
CL_x/SiO_2	6	约为 1	23.76	-	[52]
P40-750	3	约为 10	18.63	3.1×10^5	[3]
2-MWNT-sil-P	4	24	32.92	-	[53]
CPF-T-COOH	2	0.5	64.63	6.0×10^6	本研究

注：0.075-AA-0.072@MIL-101 为丙烯酸功能化的金属有机骨架材料； BT/$CoFe_2O_4$@SiO_2-CMC/PAN 为羧甲基壳聚糖和 1-(2-吡啶偶氮)-2-萘基功能化的磁性膨润土纳米材料； IIPBT/$CoFe_2O_4$@SiO_2 为离子印迹纳米复合磁性膨润土； CL_x/SiO_2 为纤维素基二氧化硅纳米复合材料； 2-MWNT-sil-P 为碳纳米管和二氧化硅复合材料。

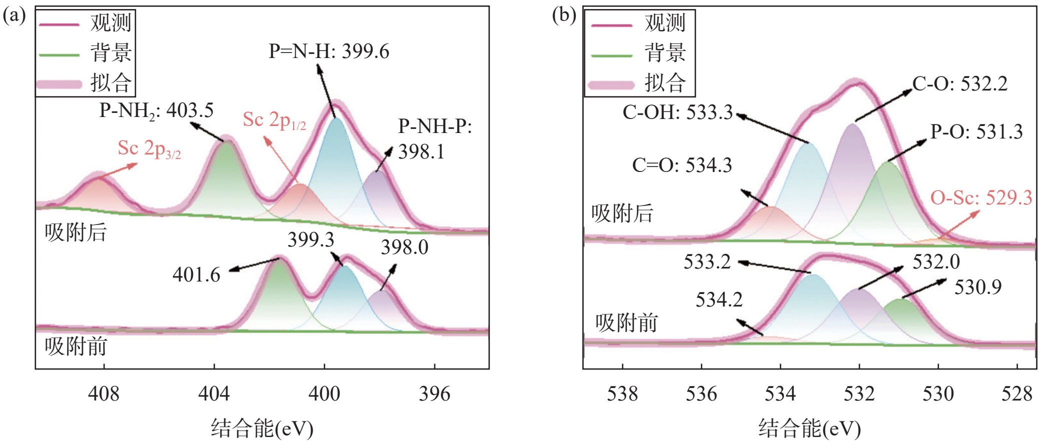

图6　CPF-T-COOH 吸附 Sc (III) 前后 N1s (a) 和 O1s (b) 高分辨 XPS 谱图

Fig. 6　High resolution XPS spectra of N1s (a) and O1s (b) before and after adsorption of Sc (III) by CPF-T-COOH.

C-O(532.0eV)[43]和 P-O(530.9eV)[24]。吸附 Sc(III)后，C=O、C-OH、C-O 和 P-O 的结合能均有所升高，偏移至 534.3eV、533.3eV、532.2eV 和 531.3eV，说明存在 O 与 Sc(III)的配位作用。值得注意的是，吸附后，O1s 的谱图中在 529.3eV 处吸附后出现了 O-Sc 的峰，同时 C-OH 的峰面积明显减小。这是因为羟基中 H 原子离去，Sc(III)与 O 形成了新的配位键[14,55]。

根据 CPF-T 和 CPF-T-COOH 的 XPS 表征结果，得到各自的 C、N、O、P 和 Cl 元素含量分别为 C：44.8%、52.9%；N：12.8%、11.8%；O：25.2%、20.8%；P：12.8%、7.3%；Cl：4.4%、7.2%。虽然在 CPF-T-COOH 中起到与 Sc(III)发生配位作用的 N、O 元素含量低于 CPF-T，但是其吸附性能更好，这可以从侧面印证多功能基团协同机制是提高对目标物吸附亲和力的有效策略。

以上结果表明，除了 CPF-T 结构中具有的 N、O 原子与 Sc(III)产生配位作用外，—COOH 提供了更多的吸附位点。—COOH 不仅通过 O 原子的配位作用固定 Sc(III)，C-OH 中的质子和 Sc(III)还存在离子交换作用。在多种机制的协同作用下，材料吸附性能得以提高。

3　结论

采用溶剂热法成功合成了 CPF-T 和富含羧基功能基团的 CPF-T-COOH。相较于 CPF-T，羧基功能化的 CPF-T-COOH 材料对 Sc(III)表现出更强的结合能力，不仅可将酸性介质中的 Sc(III)吸附效率从大约 60% 提高到 95% 以上，而且它的吸附容量是 CPF-T 的 3.5 倍。除此之外，CPF-T-COOH 对于 Sc(III)的吸附动力学得到明显改善，并且表现出更高的吸附选择性。相比于已报道的吸附剂，CPF-T-COOH 对 Sc(III)具有更广泛的 pH 适用范围。XPS 表征分析可知，CPF-T-COOH 骨架中的 P-N/P-O 和—COOH 的协同作用提高了材料在酸性介质中对 Sc(III)的吸附能力。

本研究中通过引入辅助功能基团的策略增强了吸附剂对 Sc(III)的吸附性能，为 Sc(III)的高效选择性分离提供了新材料。这项研究表明充分利用多种功能基团的协同效应是一种提高有机多孔聚合物对 Sc(III)吸附性能的有效策略，为后续高效吸附剂的设计合成提供了新思路。

Selective Separation of Scandium in Acidic Water Using Carboxyl Functionalized Covalent Phosphonitrile Polymers

BAI Yu[1,2], *WUSHUER Ayinuer*[1], *OUYANG Lei*[1], *HUANG Lijin*[1,3*], *SHUAI Qin*[1,3]
(1. Faculty of Materials Science and Chemistry, China University of Geosciences (Wuhan), Wuhan 430074, China;
2. Zhejiang Geology and Mineral Technology Co., Ltd., Hangzhou 310007, China;
3. Key Laboratory of Rare Mineral, Ministry of Natural Resources, Wuhan 430034, China)

HIGHLIGHTS

(1) Carboxyl-modified covalent phosphonitrile polymers can be used to obtain efficient and selective separation of Sc(III) in acidic media.

(2) The main interaction mechanisms between Sc(III) and —COOH modified covalent phosphonitrile polymer is coordination interaction and ion exchange.

(3) The synergistic effect of multiple functional groups effectively enhanced the binding ability of the covalent phosphonitrile polymer to Sc(III).

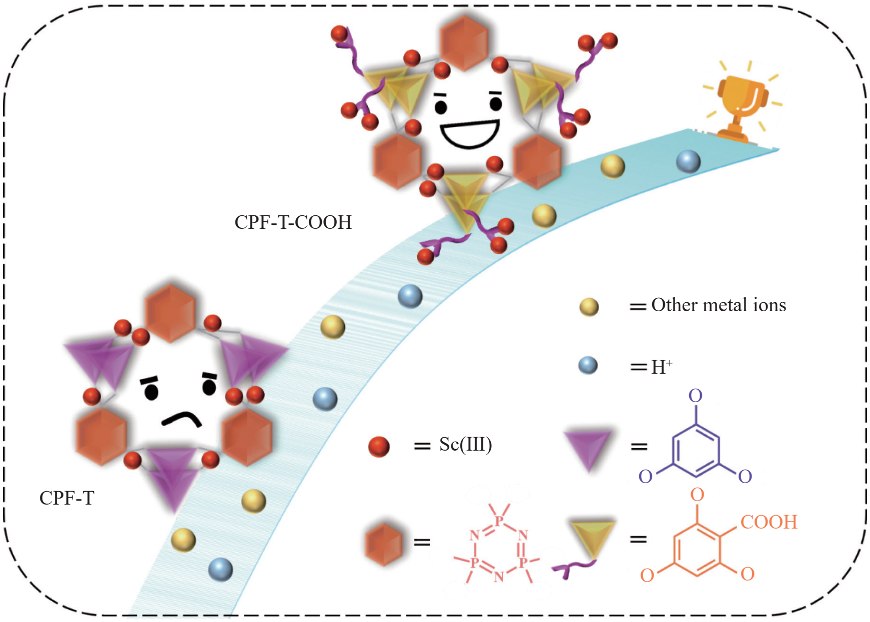

ABSTRACT

BACKGROUND: Scandium (Sc) is widely used due to its excellent properties such as high melting point, high boiling point, low density, and good stability. However, as a typical dispersed element, Sc usually exists as an associated mineral. Sc needs to be recovered from the production of ore residues and tailings by-products of other metals, the production of main products from Sc containing internal (external) deposits, or from industrial wastewater and waste residue. Among numerous technologies for separating Sc, the adsorption method exhibits promising prospects due to its advantages of simple operation and high recovery. Currently, several materials including silicon-based (such as SAB-15), biomaterials, and metal organic framework, have been used for the separation of Sc(III). Although these adsorbents exhibit good adsorption ability for Sc(III), the inherent structural drawbacks such as poor chemical stability and with only one type of functional group result in the poor selectivity and inferior adsorption capacity, thereby greatly hindering their practical applications. Considering that acid treatment is often required when processing raw materials such as Sc containing tailings, it is crucial to prepare adsorbents that can efficiently and selectively recover Sc(III) in acidic media.

Covalent organic polymers are porous organic polymer materials connected by covalent bonds. Due to their adjustable chemical structure, tunable pore size, and easy functionalization, they can be custom-made according to the characteristics of target ions. As one type of alternative adsorbents, they exhibit promising prospects. The pore size matching effect is conducive to achieving the efficient adsorption of target ions in acidic systems. However, because the pore size of the vast majority of covalent organic polymers currently synthesized is much larger than those of metal ions, this method is generally applicable to larger sized ions such as hydrated uranium ions. The utilization of ion imprinting technology or the ingenious selection of monomers with size matching cavities with the target ion to prepare covalent organic polymers are effective for address these issues. However, the complex preparation process makes it difficult to scale up. For covalent organic polymers, modification with special functional groups is another effective strategy to improve their adsorption performance. To tackle the issue of limited binding ability caused by the single functional group, research has shown that the introduction of various functional groups into the porous skeleton structure can effectively enhance the selective binding ability to target ions by utilizing the synergistic effect between different groups.

OBJECTIVES: To improve the adsorption performance of porous organic polymers for Sc(III) in acidic media by utilizing the synergistic effect of multiple functional groups.

METHODS: Phloroglucinol (1mmol) and hexachlorocyclotriphosphazene (0.5mmol) were dissolved in 1mL of 1,4-dioxane, followed by the addition of 0.84mL of triethylamine. The mixture was transferred to a hydrothermal reactor (8mL) and reacted at 80℃ for 24h. The product was washed several times with water, ethanol and acetone, respectively. Finally, CPF-T was prepared by vacuum drying at 50℃ for 12h. CPF-T-COOH was prepared according to the same procedure by changing phloroglucinol with 2,4,6-trihydroxybenzoic acid.

The infrared spectra of the CPF-T and CPF-T-COOH were collected by Thermo Scientific Nicolet iS20 Fourier transform infrared spectrometer (FT-IR) (Thermo, USA). The microstructure of the polymers was studied using SU8010 scanning electron microscope (SEM) (Hitachi, Japan). The thermogravimetric analysis (TGA) curve of the polymers was collected by the DTA7200 TGA instrument (Hitachi, Japan) under N_2 conditions (N_2 flow rate: 20mL/min; heating rate: 10K/min). The elemental information of the materials was analyzed using Thermo Scientific K-Alpha X-ray photoelectron spectrometer (XPS) (Thermo, USA). The N_2 adsorption desorption isotherm was measured at 77K using the Micromeritics APSP2460 4-station fully automatic specific surface area analyzer (Micromeritics, USA). The sample was vacuum degassed at 120℃ for 12h before measurement.

Adsorption experiments were conducted at room temperature using a constant temperature oscillator (150r/min). The adsorbent dosage was 1g/L, and the experimental data was obtained as the average of three parallel experiments. After adsorption, the supernatant was collected by filtration with 0.45μm microporous membrane. Subsequently, it was tested by EXPEC 6000 ICP-OES (Hangzhou Puyu Technology Development Co., Ltd.), and the linear correlation coefficient (R^2) of the standard curve equation was >0.999.

RESULTS: CPF-T and CPF-T-COOH were characterized by FT-IR, SEM, TGA and N_2 adsorption-desorption analysis. The appearance of P-O-Ar, P=N, and P-N stretching vibration peaks in the FT-IR diagram indicates the successful crosslinking of the organic monomers. In addition, the appearance of C=O, C-O and -OH in CPF-T-COOH indicates the successful modification of —COOH. TGA characterization indicates that the resulting materials have a good thermal stability within 150℃. Through SEM images, it can be observed that the micro morphologies of the two materials are different. CPF-T presents a relatively smooth spherical structure with some agglomerating, CPF-T-COOH exhibits an irregular, ant-like porous structure with a rough surface. The N_2 adsorption-desorption isotherms of both materials belong to type II and show a strong absorption in the range of P/P_0=0.8−1.0, indicating the presence of microporous and mesoporous structures. The specific surface area of CPF-T is 76.5m^2/g, and total pore volume is 0.38cm^3/g. The specific surface area of CPF-T-COOH is 2.61m^2/g, and the total pore volume is 0.035cm^3/g.

The adsorption performance of CPF-T and CPF-T-COOH for Sc(III) was investigated through batch adsorption experiments, including the influence of solution pH, adsorption kinetics, adsorption isotherms and adsorption selectivity. The adsorption efficiencies of Sc(III) on the two materials exhibit different trends with respect to the solution pH. As the acidity of the solution increases, the adsorption efficiency of CPF-T for Sc(III) significantly decreases, and at pH<3, the adsorption rate is below 60%. However, within the range of solution pH=1-3, the adsorption efficiency of CPF-T-COOH for Sc(III) remains above 95%. The adsorption kinetics experiment shows that CPF-T reaches adsorption equilibrium within 120min, while CPF-T-COOH can reach adsorption equilibrium within 30min. In addition, in the adsorption isotherms experiment, the maximum adsorption capacity of CPF-T-COOH (64.6mg/g) for Sc(III) was higher than that of CPF-T (22.5mg/g). Finally, the adsorption selectivity was evaluated through coexisting ion experiments. Both materials have the ability to selectively adsorb Sc(III), with K_d

values of 5.1×10^2mL/g and 4.0×103mL/g for Sc(III), respectively. The adsorption performance of CPF-T-COOH is not only higher than that of CPF-T, but also has unique advantages compared to some reported adsorbents, including a wider pH range, fast adsorption equilibrium time, and higher K_f value. These results indicate that the synergistic effect of multiple adsorption sites is an effective strategy for improving adsorption affinity of adsorbents.

The adsorption mechanism was studied through XPS analysis. In the high-resolution XPS spectrum of N1s of Sc(III) loaded sample, all the binding energies of P-NH-P(398.0eV), P=N-H(399.3eV) and P-NH_2(401.6eV) show an increase, shifting to 398.1eV, 399.6eV and 403.5eV, respectively. Meanwhile, in the spectra of O1s, it can also be observed that the binding energies of C=O(534.2eV), C-OH(533.2eV), C-O(532.0eV) and P-O(531.0eV) shift to 534.3eV, 533.3eV, 532.2eV and 531.3eV, respectively. These results indicate the existence of coordination between O/N and Sc(III). In addition, a new peak at 529.3eV corresponding to O-Sc bond appears in the spectrum of O1s for Sc(III) loading sample, and the peak area of C-OH significantly decreases. This is because the H atom in the hydroxyl group is replaced by Sc(III) through ion exchange, resulting in the formation of a new coordination bond with O.

CONCLUSIONS: Covalent phosphonitrile polymer featuring abundant carboxyl functional groups is successfully synthesized by the solvothermal method. Compared with CPF-T, the carboxyl-functionalized CPF-T-COOH exhibits a much stronger binding ability toward Sc(III), where the adsorption efficiency of Sc(III) in acidic media is greatly improved from ~60% to greater than 95%. In addition, its adsorption capacity is 3.5 times that of CPF-T. The result of the mechanism study reveals that the enhanced adsorption performance is attributed to the synergistic effect of multiple functional groups, providing an alternative route for the preparation of new materials with high adsorption performance for Sc(III) capture.

KEY WORDS: scandium (Sc); covalent phosphonitrile polymers; selective separation; synergistic effect; X-ray photoelectron spectroscopy

参考文献

[1] Barteková E, Kemp R. National strategies for securing a stable supply of rare earths in different world regions[J]. Resources Policy, 2016, 49: 153−164.

[2] Williams-Jones A E, Vasyukova O V. The economic geology of scandium, the runt of the rare earth element litter[J]. Economic Geology, 2018, 113(4): 973−988.

[3] Dai X, Thi Hong Nhung N, Hamza M F, et al. Selective adsorption and recovery of scandium from red mud leachate by using phosphoric acid pre-treated pitaya peel biochar[J]. Separation and Purification Technology, 2022, 292: 121043.

[4] Avdibegović D, Regadío M, Binnemans K. Recovery of scandium(III) from diluted aqueous solutions by a supported ionic liquid phase (SILP)[J]. RSC Advances, 2017, 7(78): 49664−49674.

[5] Yu Q, Ning S, Zhang W, et al. Recovery of scandium from sulfuric acid solution with a macro porous TRPO/SiO_2-P adsorbent[J]. Hydrometallurgy, 2018, 181: 74−81.

[6] Lu J, Li S, Tao S, et al. Efficient CO_2 electrolysis with scandium doped titanate cathode[J]. International Journal of Hydrogen Energy, 2017, 42(12): 8197−8206.

[7] Zhang W, Ning S, Zhang S, et al. Synthesis of functional silica composite resin for the selective separation of zirconium from scandium[J]. Microporous and Mesoporous Materials, 2019, 288: 109602.

[8] 杨波, 杨莉, 孟文祥. 电子探针技术探究钪在白云鄂博矿床不同矿物中的赋存特征[J]. 岩矿测试, 2022, 41(2): 185−198.
Yang B, Yang L, Meng W X. Application of electron probe microanalyzer in exploring the occurrence characteristics of scandium in different minerals of the Bayan Obo deposit[J]. Rock and Mineral Analysis, 2022, 41(2): 185−198.

[9] Hamza M F, Salih K A M, Abdel-Rahman A A H, et al. Sulfonic-functionalized algal/PEI beads for scandium, cerium and holmium sorption from aqueous solutions (synthetic and industrial samples)[J]. Chemical Engineering Journal, 2021, 403: 126399.

［10］ Rout P C, Sarangi K. A systematic study on extraction and separation of scandium using phosphinic acid by both solvent extraction and hollow fibre membrane［J］. Mineral Processing and Extractive Metallurgy, 2021, 131(2): 166−176.

［11］ Liu C, Chen L, Chen J, et al. Application of P_{507} and isooctanol extraction system in recovery of scandium from simulated red mud leach solution［J］. Journal of Rare Earths, 2019, 37(9): 1002−1008.

［12］ Ye Q, Li G, Deng B, et al. Solvent extraction behavior of metal ions and selective separation Sc^{3+} in phosphoric acid medium using P_{204}［J］. Separation and Purification Technology, 2019, 209: 175−181.

［13］ Chen Y, Ma S, Ning S, et al. Highly efficient recovery and purification of scandium from the waste sulfuric acid solution from titanium dioxide production by solvent extraction［J］. Journal of Environmental Chemical Engineering, 2021, 9(5): 106226.

［14］ Lou Z N, Xiao X, Huang M N, et al. Acrylic acid-functionalized metal-organic frameworks for Sc(III) selective adsorption［J］. ACS Applied Materials & Interfaces, 2019, 11(12): 11772−11781.

［15］ Zhang L, Chang X, Zhai Y, et al. Selective solid phase extraction of trace Sc(III) from environmental samples using silica gel modified with 4-(2-morinyldiazenyl)-N-(3-(trimethylsilyl)propyl)benzamide［J］. Analytical Chimica Acta, 2008, 629: 84−91.

［16］ Garg R, Garg R, Okon Eddy N, et al. Biosynthesized silica-based zinc oxide nanocomposites for the sequestration of heavy metal ions from aqueous solutions［J］. Journal of King Saud University-Science, 2022, 34(4): 101996.

［17］ Zhao Z, Baba Y, Yoshida W, et al. Development of novel adsorbent bearing aminocarbonylmethylglycine and its application to scandium separation［J］. Journal of Chemical Technology & Biotechnology, 2016, 91(11): 2779−2784.

［18］ Zhao R, Liao H, Wu X, et al. Selective adsorption behaviours of MOFs@SiO_2 with different pore sizes and shell thicknesses［J］. Journal of Solid State Chemistry, 2020, 292: 121693.

［19］ Liu Z, Li H. Metallurgical process for valuable elements recovery from red mud—A review［J］. Hydrometallurgy, 2015, 155: 29−43.

［20］ Borra C R, Blanpain B, Pontikes Y, et al. Recovery of rare earths and other valuable metals from bauxite residue (red mud): A review［J］. Journal of Sustainable Metallurgy, 2016, 2(4): 365−386.

［21］ Mines P D, Thirion D, Uthuppu B, et al. Covalent organic polymer functionalization of activated carbon surfaces through acyl chloride for environmental clean-up［J］. Chemical Engineering Journal, 2017, 309: 766−771.

［22］ Fan L, Duan H L, Wang J, et al. Preparation of fluorinated covalent organic polymers at room temperature for removal and detection of perfluorinated compounds［J］. Journal of Hazardous Materials, 2021, 420: 126659.

［23］ Ravi S, Kim S Y, Bae Y S. Novel benzylphosphate-based covalent porous organic polymers for the effective capture of rare earth elements from aqueous solutions［J］. Journal of Hazardous Materials, 2022, 424: 127356.

［24］ Zhang M, Li Y, Bai C, et al. Synthesis of microporous covalent phosphazene-based frameworks for selective separation of uranium in highly acidic media based on size-matching effect［J］. ACS Applied Material & Interfaces, 2018, 10(34): 28936−28947.

［25］ Li X, Qi Y, Yue G, et al. Solvent- and catalyst-free synthesis of an azine-linked covalent organic framework and the induced tautomerization in the adsorption of U(Ⅵ) and Hg(II)［J］. Green Chemistry, 2019, 21(3): 649−657.

［26］ Huang J, Cui W R, Wang Y G, et al. Rational designed molecularly imprinted triazine-based porous aromatic frameworks for enhanced palladium capture *via* three synergistic mechanisms［J］. Chemical Engineering Journal, 2022, 430: 132962.

［27］ Zhang W, Wang S, Cao X, et al. A facile coordinate complexing of Na(I) to fabricate SPB-ACE@MS-4A for selective adsorption to monovalent alkali metal ions［J］. Desalination, 2021, 520: 115337.

［28］ Huang L J, Shen R J, Liu R Q, et al. Thiol-functionalized magnetic covalent organic frameworks by a cutting strategy for efficient removal of Hg^{2+} from water［J］. Journal of Hazardous Materials, 2020, 392: 122320.

［29］ 周慧君, 帅琴, 黄云杰, 等. 双硫腙改性氧化石墨烯/壳聚糖复合微球固相萃取在线富集-原子荧光光谱法测定地质样品中痕量汞[J]. 岩矿测试, 2017, 36(5): 474−480.

Zhou H J, Shuai Q, Huang Y J, et al. On-line determination of Hg(II) in geological samples by afs after solid phase extraction using dithizone-modified graphene oxide/chitosan composite microspheres［J］. Rock and Mineral Analysis, 2017, 36(5): 474−480.

［30］ Ravi S, Puthiaraj P, Yu K, et al. Porous covalent organic polymers comprising a phosphite skeleton for aqueous Nd(III) capture[J]. ACS Applied Materials & Interfaces, 2019, 11(12): 11488−11497.

[31] 赵亮, 李嘉权, 王岩, 等. 氨基改性 Cu-BTC 对水溶液中镧铈稀土离子的吸附研究[J]. 石油化工, 2023, 52(4): 469−477.
Zhao L, Li J Q, Wang Y, et al. Adsorption of rare earth ions la and ce from aqueous solution by amino-modified Cu-BTC[J]. Petrochemical Technology, 2023, 52(4): 469−477.

[32] Xie Y, Wu Y, Liu X, et al. Rational design of cooperative chelating sites on covalent organic frameworks for highly selective uranium extraction from seawater[J]. Cell Reports Physical Science, 2023, 4(1): 101220.

[33] Liu M, Chen J, Zou D, et al. A novel synergistic extraction system for the recovery of scandium(III) from sulfuric acid medium with mixed cyanex923 and N1923[J]. Separation and Purification Technology, 2022, 283: 120223.

[34] Hu Z P, Jiang H L, Hu Q D, et al. Preparation of the hexachlorocyclotriphosphazene crosslinked sodium alginate polymer/multi-walled carbon nanotubes composite powder for the removal of the cationic dyes[J]. Journal of Molecular Structure, 2022, 1262: 133050.

[35] Lv M, Yao C, Yang D, et al. Synthesis of a melamine-cyclotriphosphazene derivative and its application as flame retardant on cotton gauze[J]. Journal of Applied Polymer Science, 2016, 133(25): 43555.

[36] Mohamed M G, Hsiao C H, Luo F, et al. Multifunctional polybenzoxazine nanocomposites containing photoresponsive azobenzene units, catalytic carboxylic acid groups, and pyrene units capable of dispersing carbon nanotubes[J]. RSC Advances, 2015, 5(56): 45201−45212.

[37] Liu R, Yan Q, Tang Y, et al. Nacl Template-assisted synthesis of self-floating COFs foams for the efficient removal of sulfamerazine[J]. Journal of Hazardous Materials, 2022, 421: 126702.

[38] Xu S, Weng Z, Tan J, et al. Hierarchically structured porous organic polymer microspheres with built-in Fe_3O_4 supraparticles: Construction of dual-level pores for Pt-catalyzed enantioselective hydrogenation[J]. Polymer Chemistry, 2015, 6(15): 2892−2899.

[39] Ma Z, Liu F, Liu N, et al. Facile synthesis of sulfhydryl modified covalent organic frameworks for high efficient Hg(II) removal from water[J]. Journal of Hazardous Materials, 2021, 405: 124190.

[40] Chen Y, Wang S, Li Y, et al. Adsorption of Pb(II) by tourmaline-montmorillonite composite in aqueous phase[J]. Journal of Colloid and Interface Science, 2020, 575: 367−376.

[41] Wang P, Ding F, Huang Z, et al. Adsorption behavior and mechanism of Cd(II) by modified coal-based humin[J]. Environmental Technology & Innovation, 2021, 23: 101699.

[42] Wood S A, Samson I M. The aqueous geochemistry of gallium, germanium, indium and scandium[J]. Ore Geology Reviews, 2006, 28(1): 57−102.

[43] Zhang L, Wang C, Yang R, et al. Novel environment-friendly magnetic bentonite nanomaterials functionalized by carboxymethyl chitosan and 1-(2-pyridinylazo)-2-naphthaleno for adsorption of Sc(III)[J]. Applied Surface Science, 2021, 566: 150644.

[44] Salman A D, Juzsakova T, Akos R, et al. Synthesis and surface modification of magnetic Fe_3O_4@SiO_2 core-shell nanoparticles and its application in uptake of scandium(III) ions from aqueous media[J]. Environmental Science Pollution Research, 2021, 28(22): 28428−28443.

[45] Wang J, Guo X. Adsorption kinetic models: Physical meanings, applications, and solving methods[J]. Journal of Hazardous Materials, 2020, 390: 122156.

[46] Xu W, Zhou S, Wang B, et al. Efficient adsorption of Au(III) from acidic solution by a novel N, S-containing metal–organic framework[J]. Separation and Purification Technology, 2022, 288: 120646.

[47] 杨梦楠, 孙晗, 曹海龙, 等. 生物炭-壳聚糖磁性复合吸附的制备及去除地下水中铅和铜[J]. 岩矿测试, 2023, 42(3): 563−575.
Yang M N, Sun H, Cao H L, et al. Preparation and application of biochar-chitosan magnetic composite adsorbent for removal of lead and copper from groundwater[J]. Rock and Mineral Analysis, 2023, 42(3): 563−575.

[48] Wang J, Guo X. Adsorption isotherm models: Classification, physical meaning, application and solving method[J]. Chemosphere, 2020, 258: 127279.

[49] Li X, Liu Z, Wei L, et al. Comparison of competitive and synergistic adsorption of tetrabromobisphenol-A and its metabolites on two different organic-modified clays[J]. Journal of Chemical & Engineering Data, 2019, 64(6): 2780−2790.

[50] Tran H N, Bonilla-Petriciolet A. Improper estimation of thermodynamic parameters in adsorption studies with distribution coefficient K_d (Q_e/C_e) or Freundlich constant

(K_f): Considerations from the derivation of dimensionless thermodynamic equilibrium constant and suggestions[J]. Adsorption Science & Technology, 2022, 2022: 1−23.

[51] Wang C, Zhang L, Zhou G, et al. Synthesis of environmental-friendly ion-imprinted magnetic nanocomposite bentonite for selective recovery of aqueous Sc(III)[J]. Journal of Colloid and Interface Science, 2023, 630: 738−750.

[52] Iftekhar S, Srivastava V, Sillanpää M. Enrichment of lanthanides in aqueous system by cellulose based silica nanocomposite[J]. Chemical Engineering Journal, 2017, 320: 151−159.

[53] Ramasamy D L, Puhakka V, Doshi B, et al. Fabrication of carbon nanotubes reinforced silica composites with improved rare earth elements adsorption performance[J]. Chemical Engineering Journal, 2019, 365: 291−304.

[54] Wu J S, Li Z, Tan H X, et al. Highly selective separation of rare earth elements by Zn-Btc metal-organic framework/nanoporous graphene *via in situ* green synthesis[J]. Analytical Chemistry, 2021, 93(3): 1732−1739.

[55] 王哲, 朱俊, 李雯, 等. 镧沸石对磷和重金属的吸附与底泥钝化性能[J]. 环境科学, 2022, 43(11): 5106−5114.
Wang Z, Zhu J, Li W, et al. Adsorption of phosphate and heavy metals by lanthanum modified zeolite and its performance in sediment inactivation[J]. Environmental Science, 2022, 43(11): 5106−5114.

[56] He J, Lu Y, Luo G. Ca(II) imprinted chitosan microspheres: An effective and green adsorbent for the removal of Cu(II), Cd(II) and Pb(II) from aqueous solutions[J]. Chemical Engineering Journal, 2014, 244: 202−208.

[57] Gao X, Zhang Y, Zhao Y. Biosorption and reduction of Au(III) to gold nanoparticles by thiourea modified alginate[J]. Carbohydrate Polymers, 2017, 159: 108−115.